Spectral Diffraction Efficiency Characterization of Broadband Diffractive Optical Elements

Junoh Choi, Alvaro A. Cruz-Cabrera, Anthony Tanbakuchi

ⓕ Sandia National Laboratories

Spectral Diffraction Efficiency Characterization of Broadband Diffractive Optical Elements

Junoh Choi (5712), Alvaro A. Cruz-Cabrera (1535), Anthony Tanbakuchi (5717)

Sandia National Laboratories
P.O. Box 5800
Albuquerque, New Mexico 87185-MS0406

Abstract

Diffractive optical elements, with their thin profile and unique dispersion properties, have been studied and utilized in a number of optical systems, often yielding smaller and lighter systems. Despite the interest in and study of diffractive elements, the application has been limited to narrow spectral bands. This is due to the etch depths, which are optimized for optical path differences of only a single wavelength, consequently leading to rapid decline in efficiency as the working wavelength shifts away from the design wavelength. Various broadband diffractive design methodologies have recently been developed that improve spectral diffraction efficiency and expand the working bandwidth of diffractive elements. We have developed diffraction efficiency models and utilized the models to design, fabricate, and test two such extended bandwidth diffractive designs.

CONTENTS

FIGURES

NOMENCLATURE

RMS   Root mean square
PSF   Point spread function
HeNe   Helium Neon
Ti:Sapphire   Titanium Sapphire

1. INTRODUCTION

Space-based optical payloads are designed and fabricated to perform in harsh thermal and radiation environments. These unique environments limit the choice of optical materials as they need to be radiation resistant, withstand mechanical forces of launch, and have broad spectral transmission. The limited number of radiation resistant optical materials removes degrees of freedom to correct aberrations and the consequence is that space-based optical systems tend to be heavy, more sensitive to alignment errors and complex with many optical and mechanical elements.

Diffractive optical elements, with their thin profile and unique dispersion properties, have been studied and utilized in a number of optical systems, often yielding smaller and lighter systems. Diffractive optical elements are components that redirect light by altering the wavefront of subsections of a beam and stitching them as the wavefront propagates away from the device. The stitching occurs because the optical path difference imparted by each subsection is an integer multiple of the working wavelength. The zone spacing of a diffractive element can be designed to add a focusing or even an aspheric term to an incident wavefront. The depths of diffractives are much smaller than refractive element sags and lead to thinner profile components. However, although diffractive elements are thinner than the traditional refractive lenses, the use of diffractives has been limited to narrow spectral bands due to rapid loss of diffraction efficiency at non-design wavelengths as shown in Figure 1.

Conventional Optimized Efficiency Diffractive Element
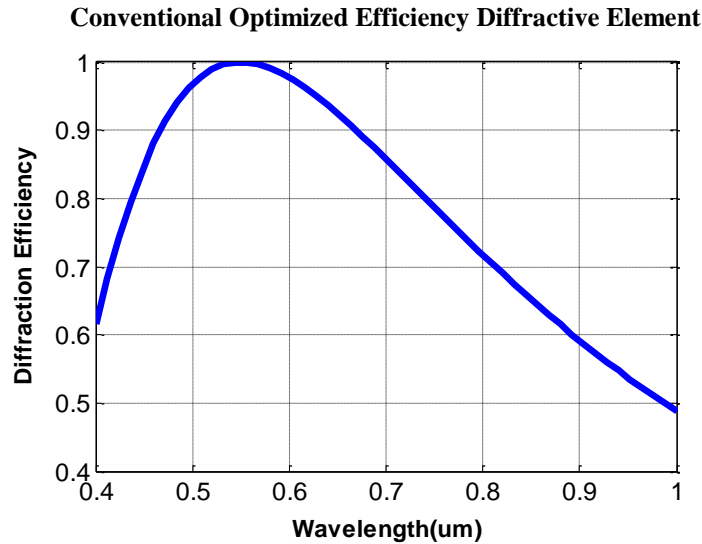
Figure 1. Theoretical diffraction efficiency of an optimized efficiency diffractive element. (Blazed diffractive element)

Recent efforts[1,2] to expand the working spectral bandwidth of diffractive elements have led to design methodologies that improve the diffraction efficiency over a larger range of wavelengths. Multi-layer diffractive and the harmonic, or multi-order, diffractive designs are two examples of such broadband diffractive designs. Spectral transmission is an important parameter that needs to be understood for a broadband optical system and if a broadband diffractive element is to be

incorporated into a broadband system, then the diffractive element's spectral diffraction efficiency will need to be well characterized.

In this paper we present results from design, efficiency modeling, and fabrication of the two aforementioned broadband diffractive element designs. The diffractive elements were fabricated with fused silica and calcium fluoride by grayscale lithography and diamond turning, respectively. We also present results from spectral diffraction efficiency measurements of the fabricated broadband diffractive elements.

2. DESIGN & MODELING

Design considerations for a diffractive lens are in some aspects similar to those of a traditional lens in that typical raytrace software can be used to design a diffractive element's optical power, clear aperture, and the material. These typical optical parameters then translate to zone spacings, and number of zones in a clear aperture for a diffractive element. Another parameter that needs to be modeled and specified for a diffractive is the step height of the diffraction surface that determines the diffraction efficiency of the designed orders. We modeled the spectral diffraction efficiencies of the two broadband design methods to determine the desired depths of the diffractive designs. Also, to ensure manufacturability of the designed diffractive elements, we performed a survey of the manufacturing industry and put together a loose set of guidelines – due to lack of a clear set of limitations – for fabrication limits for lithography on fused silica and diamond turning calcium fluoride.
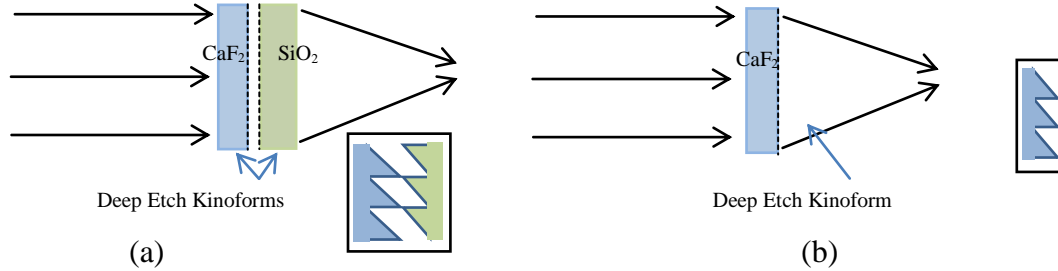
Figure 2. (a) Depicts the "efficiency achromatized" (multi-layer) diffractive design and (b) depicts the multi-order (harmonic) diffractive design

2.1. Efficiency model of the harmonic diffractive design

The multi-order diffractive element does not actually broaden the efficiency at a given wavelength but provides multiple wavelengths where the efficiency is high with a diffraction angle identical to the diffraction angle at the design wavelength. This device differs from the multi-layer diffractive element by using only one material. Its depths are integer multiples of the optimized depth for a conventional diffractive:

$$d_h = p \frac{\lambda_0}{n_0 - 1} \tag{1}$$

10

Where p is an integer that denotes the harmonic (p is 1 in standard diffractives), λ_0 is the design wavelength, and n_0 is the refractive index at the design wavelength. By increasing the depth by integer multiples the harmonic diffractive allows adjacent orders to provide near unity efficiencies at different wavelengths. The efficiencies are calculated using reference 2:

$$\eta = \sum e^{-i\pi(\alpha p - m)} sinc(\alpha p - m) e^{\left(\frac{-i\pi m r^2}{p \lambda_0 F_0}\right)} \quad and \quad \alpha = \frac{\lambda_0}{\lambda}\left(\frac{n(\lambda)-1}{n(\lambda_0)-1}\right), \tag{2}$$

where α is the 2π phase delay for wavelengths other than the intended wavelength, m is the diffraction order and F_0 is the focal length for the design wavelength. Figure 3 shows a 2D description of the efficiencies of the diffractives. White is efficiency close to 1 and black is zero efficiency. The y-axis is the wavelength range for the analysis of the harmonic design, and the x-axis is the diffractive order. Notice that at 0.55µm the utilized order is 20. This is the case we are trying to fabricate with a depth of 25.32µm and a minimum zone width to depth ratio of 22.48:1, which is well within the advised fabrication limits of current fabrication methods.
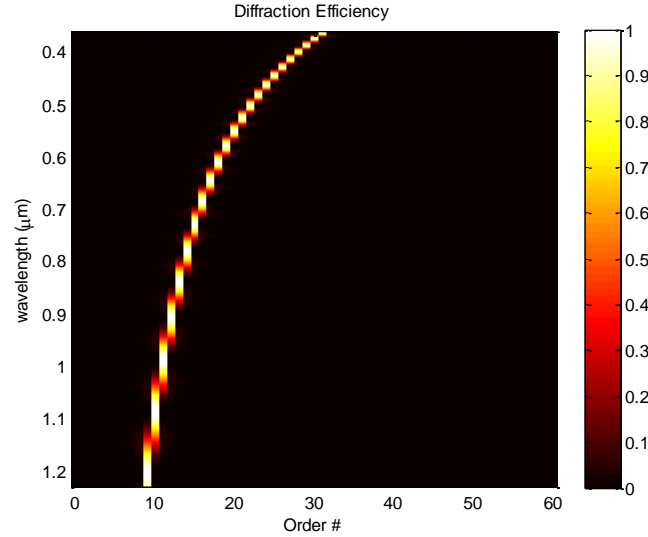
Figure 3. Shows diffraction efficiency of the multi-order diffractive as function of the order number (x-axis) and its wavelength (y-axis). White is an efficiency of 1 and black is an efficiency of 0. The graph shows that as the wavelength gets shorter the order numbers with high efficiency increase.

Another aspect that needs to be addressed in this type of device is the sparsity of high efficiency orders; see Figure 4(a) for p= 20. With deeper structures we can increase the number of higher efficiency orders; see Figure 4(b) for p= 40. These two figures show the efficiency (y-axis) for each order (each one has a different color) versus wavelength (x-axis). The example in Figure 4(b) show that the orders with high diffraction efficiency are more closely packed when the design uses more harmonics, and consequently the device gets deeper.
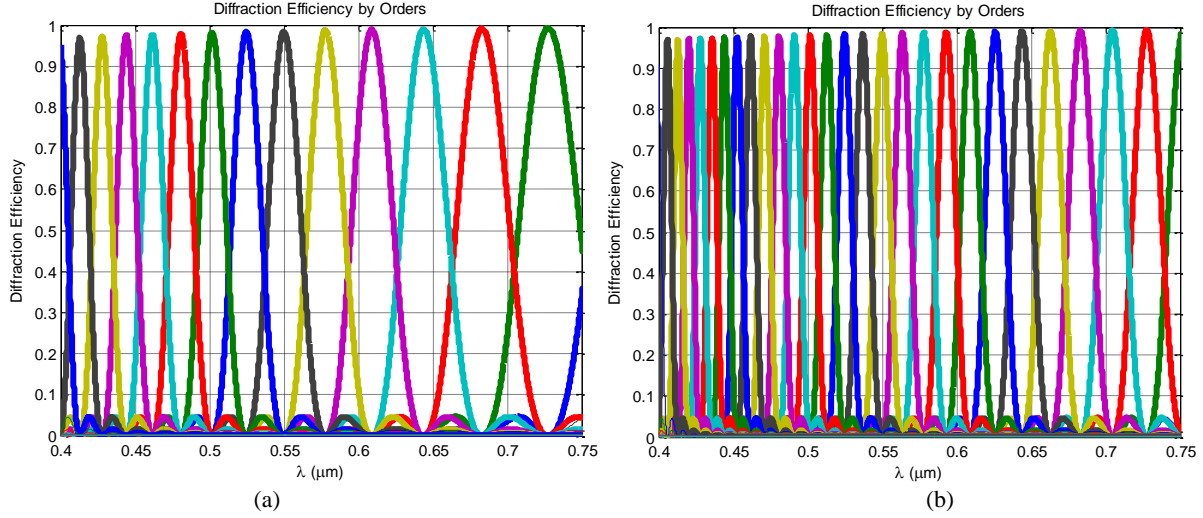
Figure 4. Graph shows the efficiency of harmonic diffractive for all possible orders and no limitation in acceptance angle. Panel (a) shows the case where p= 20 is used to define an etch depth of 25.31µm, but providing ample separation between the peak efficiency of each order, and where the diffraction angles are close but not identical due to dispersion. Panel (b) shows the case where p= 40 is used to define an etch depth of 50.61µm, while providing a closer separation between the peak efficiency of the orders. Each color is an order that peaks its efficiency at different wavelength.

It can also be determined from the grating equation $sin\theta = p^{\lambda}/_{\Lambda}$, (where Λ is the period) that each order at its peak efficiency will diffract at the same angle as the other orders. Figure 5(a) shows that behavior for a material without dispersion. However with real material, dispersion needs to be accounted as the focal point changes with the order, see Figure 5(b).
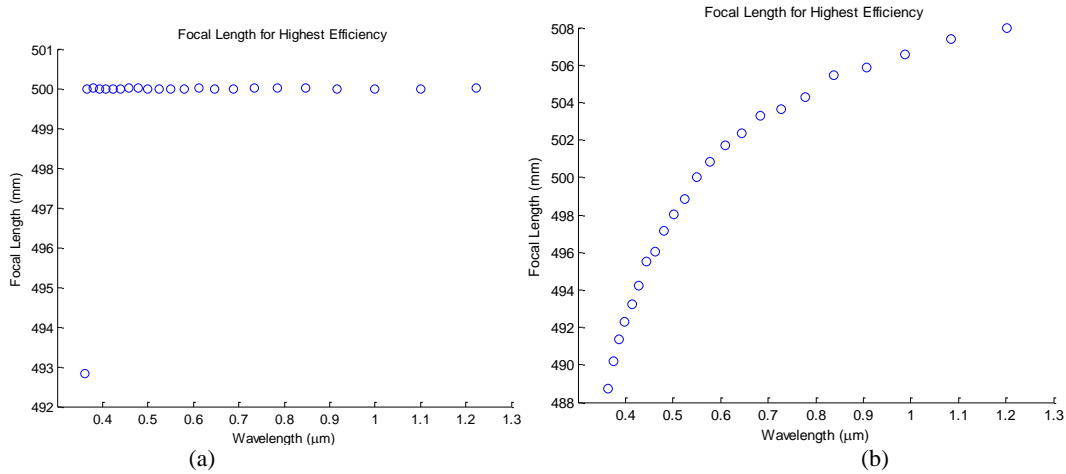
Figure 5. Focal length for (a) an ideal case where there is no material dispersion and (b) with measured dispersion, in this case of calcium fluoride. Each of the dots in the curves corresponds to the highest efficiency of an order. The leftmost point from panel (a) is an artifact of the calculation, as it is at the boundary of the measured dispersion for calcium fluoride.

A perfect theoretical harmonic diffractive element will restrict diffraction angle to the calculated diffraction angle, and that will limit the amount of light being accepted; see Figure 6(a). If the

12

acceptance angle is wider, then the system will seem to provide a better efficiency response; see Figures 6(b) and (c). However, the spot size at the focal plane will be degraded.
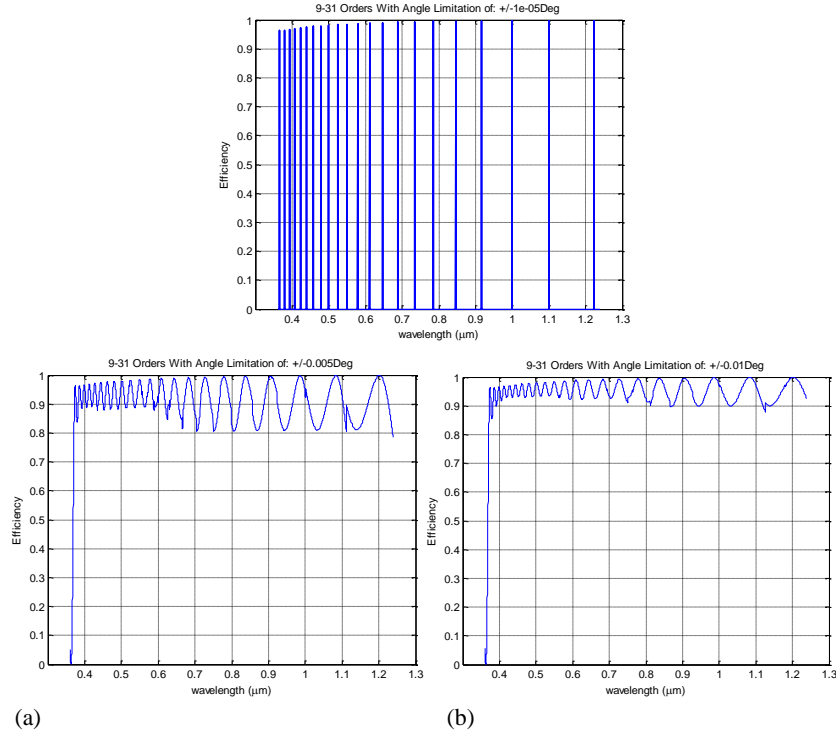
Figure 6. Panel (a) shows the diffraction efficiency for a 20 harmonic diffractive design in the visible range with limitations in the acceptance angle of +/- 0.00001 Degrees (this number is used for demonstration purposes). Panel (b) shows the same design but restricting its acceptance angle to +/- 0.005 Degrees. Panel (c) shows a restriction to an acceptance angle of +/-0.01 Degrees.

2.2. Efficiency model of the multi-layer diffractive design

Unlike the harmonic design, the multi-layer diffractive design broadens the spectral diffraction efficiency by using two materials with different dispersion properties. Each substrate has a deep etch diffractive on one side, facing each other where the two kinoforms have complementary surface profiles. The addition of a second material provides two additional degrees of freedom - the depth of the second kinoform and its dispersion - that modify the spectral efficiency of the combined system to provide two peaks. The phase change induced by the two complementary kinoforms is[1]:

$$\Phi(\lambda) = \frac{2\pi h_1}{\lambda}(n_1(\lambda) - 1) - \frac{2\pi h_2}{\lambda}(n_2(\lambda) - 1), \tag{3}$$

where n_1 and n_2 are the refractive indices of the materials, h_1 and h_2 are the depths of the respective kinoforms, and the λ is the wavelength. This equation assumes that the devices are working at scalar regimes (the periods are at least 10 times larger than the working wavelength).
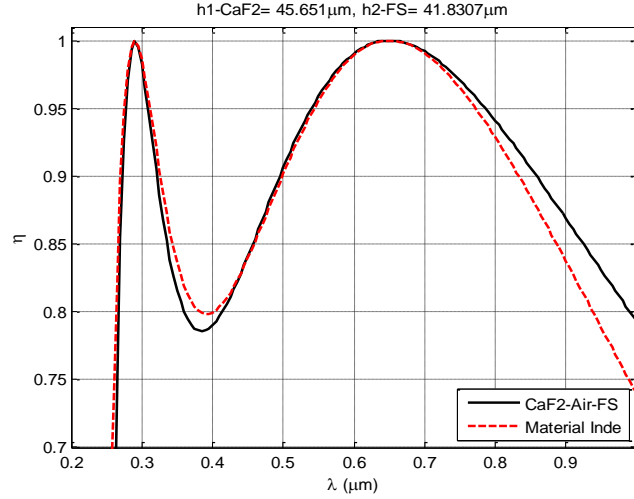
Figure 7. Curves show generic prediction of efficiency for multi-layer design with two design wavelengths of 0.290µm and 0.65µm. This design solution clearly shows the two efficiency peaks.

Figure 7 shows an example of a non-optimal but illustrative design showing two peaks in the diffraction efficiency of the multi-layer element. The red curve is the calculated efficiency using the dispersion of fused silica and calcium fluoride, the black curve comes from a derived equation[1] that is independent of the material. The example in Figure 7, however, requires diffractive elements with depths greater than 40 microns. With the zone widths for the particular design we were considering, the depth did not yield a manufacturable design. We modified the design to come as close to the current fabrication limitations as possible which resulted in the diffraction efficiency curve to have a closely placed peak wavelengths at 0.35um and 0.4um. See Figure 8.
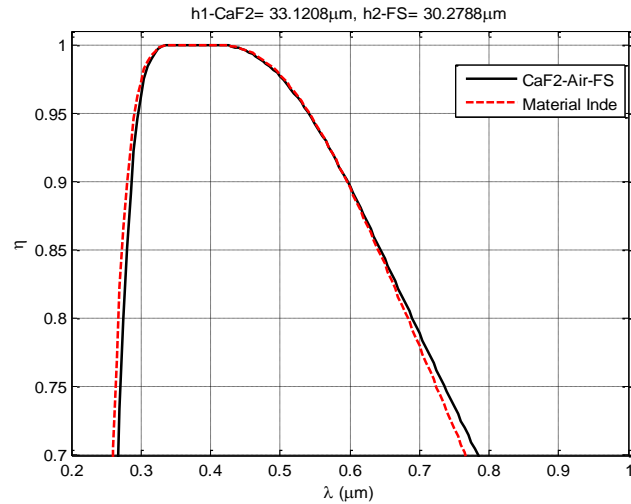
Figure 8. Prediction of the efficiency response of the multi-layer diffractive design. The red curve is the calculated response using the dispersion of fused silica and calcium fluoride, the black curve comes from the equation that is independent to material. The flat top is the location for the two wavelength peak designs of 0.35µm and 0.4µm.

This narrow band was selected for the fused silica substrate etch-depth of 30.28µm and 33.12µm for calcium fluoride. The minimum zone width and the step height ratio of the final multi-layer diffractive design had a ratio of 7.6:1 for fused silica, a 6.97:1 ratio for calcium fluoride.

3. FABRICATION

One component of the multi-layer diffractive was fabricated using grayscale lithography with fused silica as the substrate material. The complementary diffractive component as well as the harmonic diffractive element was diamond turned on calcium fluoride. The as-built multi-layer diffractive element had a clear aperture diameter of 14mm and the harmonic diffractive element had a clear aperture diameter of 20mm. After receiving the manufactured components, they were examined and the 1-D surface profiles were compared to their respective design values. Results from the surface profile measurements with a Dektak profilometer of a lithographically etched diffractive and a diamond-turned diffractive are shown below. It should be noted that the profilometry was done with a probe tip with a diameter of 2 microns and the diamond turning tool tip had a diameter of 25 microns. Also, the results shown are for two different diffractive designs where the step height and the zone widths, as well as the clear aperture and the total number of zones, differ.

3.1. Surface profile of a diamond-turned component

The surface profile shown in Figure 9 is of the diamond turned component designed as the harmonic diffractive. Some of the fabrication errors observed are the step height error, the zone spacing error, and the zone transition error. Figure 9 shows the surface profile comparison of the as-built against the design. The error in the step height in the central zone is approximately 4%. The zone depth as well as the zone spacing shows radial variation where the error appears to slightly grow with the radius. At the location of the last zone, the depth error is as great as 10% and the zone spacing error is approximately 1 micron.
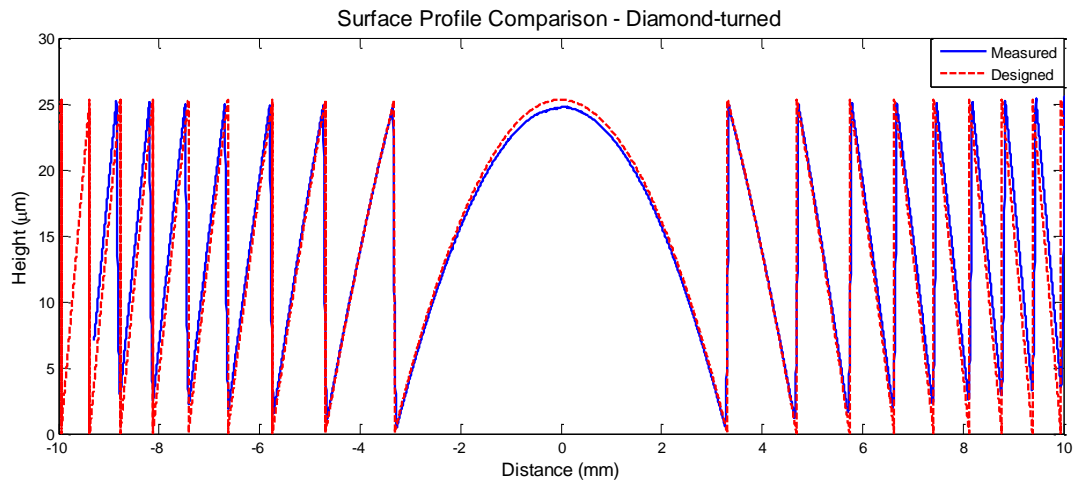
Figure 9. Surface profile of the diamond-turned harmonic DOE in calcium fluoride

15

Plots included in Figure 10 show surface roughness in the central zone of the diamond-turned element and a region of a zone transition. As expected, the zone transition shows sloped boundary with a rounded corner.

(a)

(b)
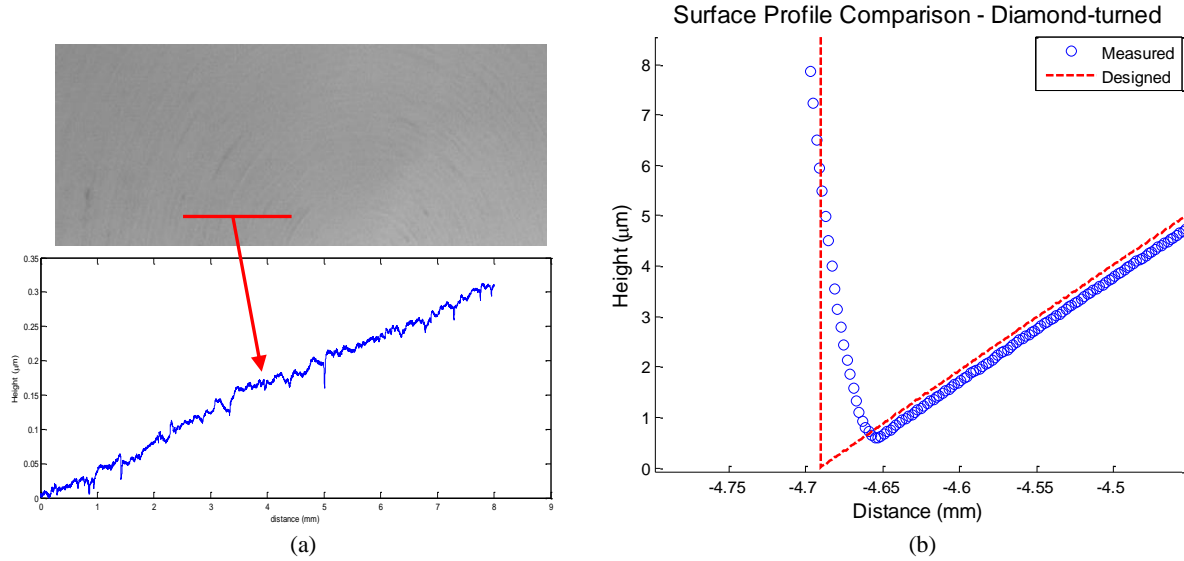
Figure 10. Results from surface profilometry of the diamond-turned diffractive element showing (a) surface roughness, and (b) zone transition error.

The surface profilometry data was used to calculate the RMS surface error of the diamond-turned element for the central zone region. The RMS surface roughness was calculated from the profile data after removing the surface figure with a best-fit 8th order polynomial from the measured data. Close-up view of the data from the central zone clearly captures the slight discontinuity at the center of the component. See Figure 11. The RMS surface error calculated from the data is 0.014 microns. Using the following approximation for total integrated scatter[3],

$$TIS \approx \left(\frac{2\pi\sigma\Delta n}{\lambda}\right)^2, \tag{4}$$

where σ is the RMS surface roughness, Δn is the difference in refractive indices, the estimated scatter from surface roughness is about 0.4% at 600nm and 0.31% at 700nm. It can be expected from the power spectral density plot in Figure 11(c) that most of that scatter will happen at small angles near the specular ray.
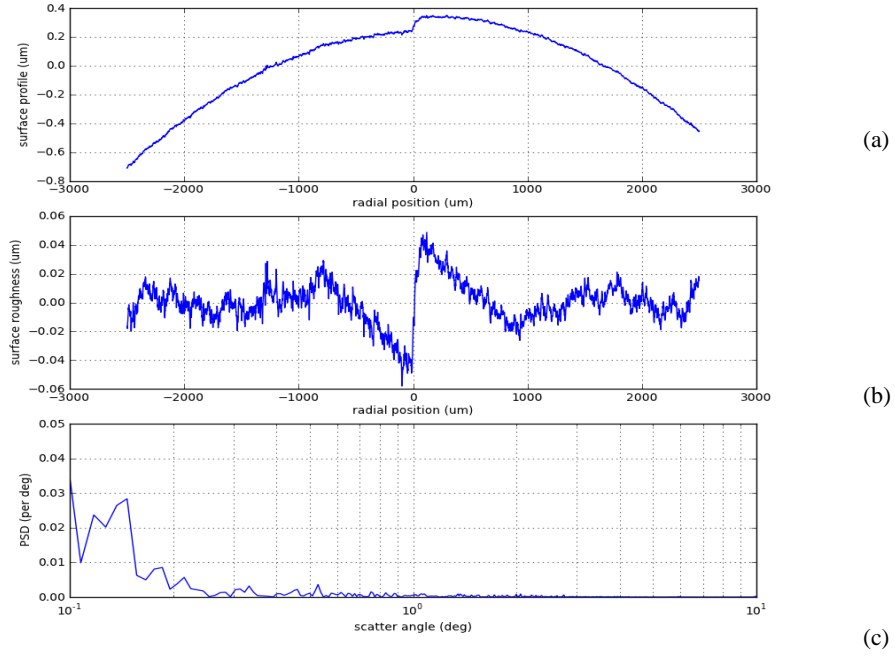
Figure 11. Results from surface profilometry of the diamond-turned diffractive element showing (a) surface profile, (b) surface roughness, and (c) power spectral density plot.

3.2. Surface profile of a grayscale lithographed component

The grayscale diffractive element also showed some error in the etch depth which was measured at approximately 4% and as great as 8% near the edge of the clear aperture. Surface profile plots of the measured versus the design is shown in Figure 12. Errors in zone spacings are measured to be as great as 20nm.
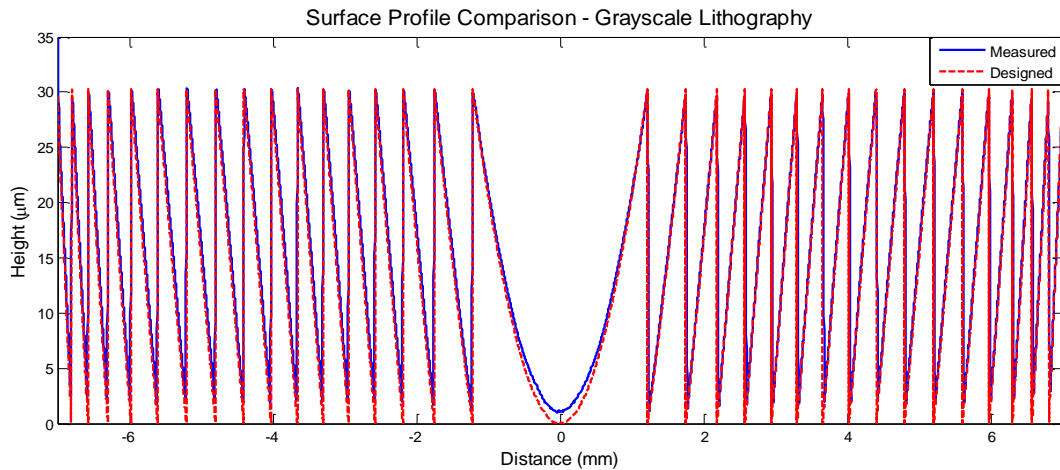
Figure 12. Surface profile of lithographically etched diffractive element.

An interesting feature that was captured during the inspection with the profilometer is the corrugation in the central zone of the element which we suspect is an artifact of the error present in the mask. An image of a region in the central zone is shown in Figure 13 (a) with a surface plot clearly depicting the linear features.

(a)   (b)
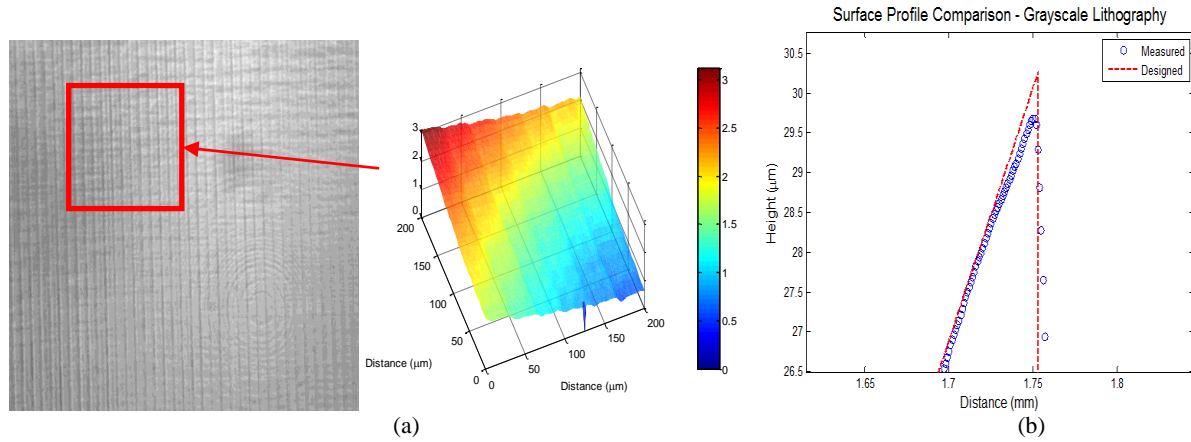
Figure 13. Results from the surface profilometry showing (a) corrugation in the central zone and (b) zone transition error.

Figure 14 shows a surface profile plot, a surface roughness plot, and a power spectral density. The surface roughness was calculated the same way it was done for the diamond-turned optic and the calculated RMS error was 0.038 microns for the lithographed component. From the RMS value, the estimated scatter is 3.3% at 600nm and 2.4% at 700nm. The power spectral density plot shows that the grayscale element will have scattered light that is mostly directed in angles near 1 degree and 2 degrees.
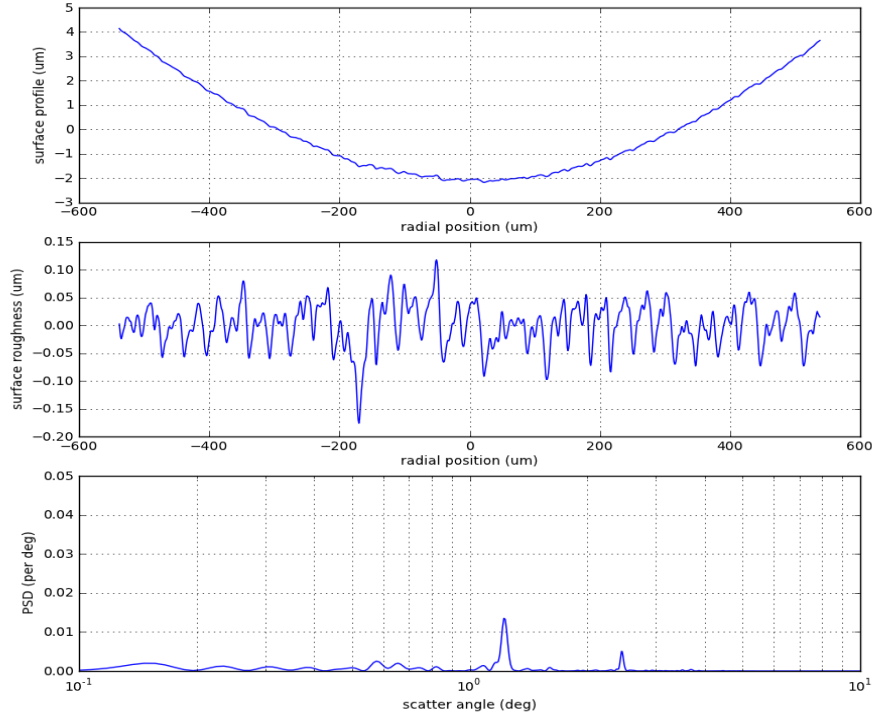
Figure 14. Results from surface profilometry of the lithographically etched component showing (a) surface profile, (b) surface roughness, and (c) power spectral density.

4. DIFFRACTION EFFICIENCY MEASUREMENTS

4.1. Measured efficiency of the harmonic diffractive element

Transmittance is a property of a material defined as the fraction of the incident light that passes through the material. For a lens with focusing power, the transmittance of the lens material determines how much energy passes to the image plane and the aberration content of the lens governs how that energy is distributed. Transmittance of an optical component can be measured by taking the ratio of the output versus the input power and is affected by surface scatter, Fresnel reflection, bulk absorption, and bulk scatter. Equation 5 shows how the total transmittance is related to the aforementioned parameters. The equation also includes a coefficient for diffraction efficiency, which is assumed to be perfect for a refractive lens.

$$\frac{P_{out}}{P_{in}} = T = T_{DE} \cdot T_{ss} \cdot T_{FR} \cdot T_{BA} \cdot T_{BS} \tag{5}$$

For thin optical elements − lenses used in our tests were all less than 5mm in thickness − the transmission losses due to bulk scatter and bulk absorption are negligible. Fresnel reflection loss can be easily calculated with the refractive index information and surface scatter can be

estimated using the rms surface roughness. For our tests, however, the input power of the laser was measured before the collimator where the beam diameter was still small, resulting in lower power measurements due to losses from the collimator. To eliminate the losses from the collimator, the transmittance measurement of the test diffractive optic was normalized by the transmittance measurement of a reference refractive lens. The test and the reference optics both have the same F-number and use the same collimator. Since a refractive lens has a "diffraction efficiency" of 1, the ratio of the transmittance values give us a diffraction efficiency value without the losses from other optical elements in the test configuration.
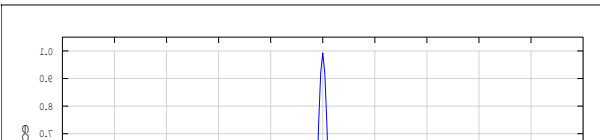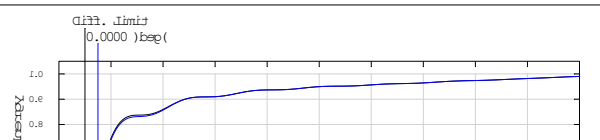
$$\text{Efficiency} = \frac{T_{DOE}}{T_{Lens}} = \frac{T_{DE} \cdot T_{ss} \cdot T_{FR} \cdot T_{BA} \cdot T_{BS} \cdot T_{other}}{1 \cdot T_{ssL} \cdot T_{FRL} \cdot T_{BAL} \cdot T_{BSL} \cdot T_{other}} \qquad (6)$$

The designed harmonic diffractive element was an f/25 lens where optical modeling software, ignoring diffraction efficiency, simulated a diffraction limited performance. We identified Newport's SPX031 lens as a reference refractive lens with a comparable focal length lens and added an aperture to operate it at f/25. Both the harmonic diffractive and the refractive lens were uncoated singlets. Our method of measuring the diffraction efficiency involved collimating a laser source and measuring power at the focal plane of the harmonic element. P_{in}/P_{out} ratio for the harmonic element was then normalized by the same P_{in}/P_{out} ratio measured with the reference refractive lens. We call this normalized ratio the measured diffractive efficiency in this paper. Figure 15 shows the layout of the optical bench test setup.
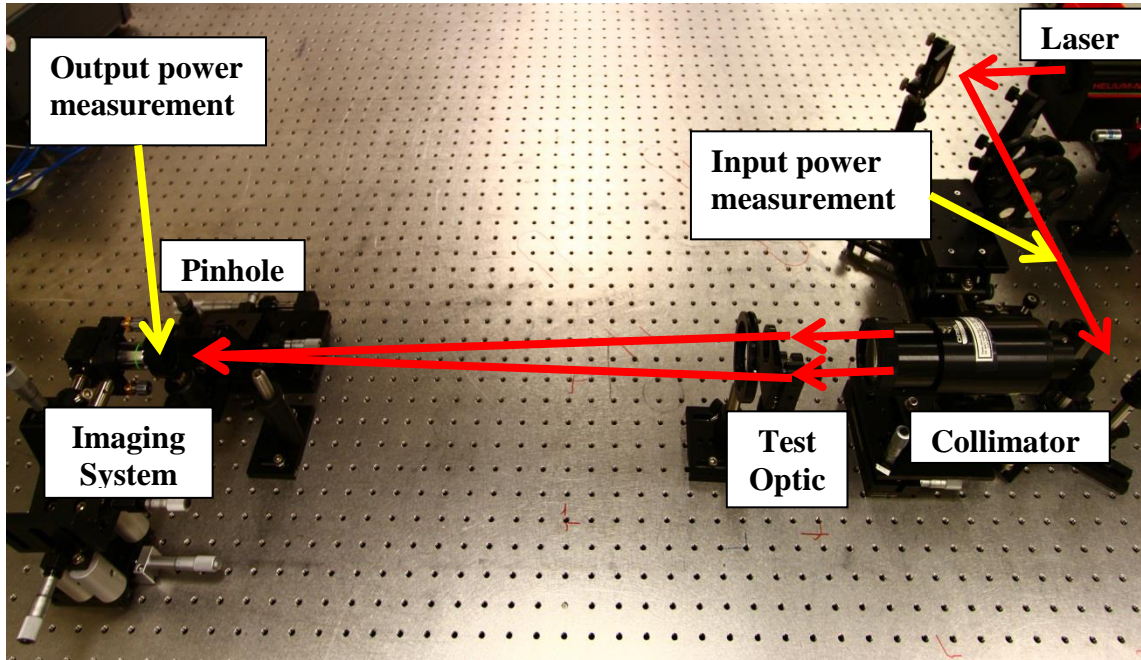
Figure 15. Layout of the experimental setup

Isolating power from the desired order from light from other orders was a critical step in these measurements. Both the harmonic diffractive and the reference refractive lens were diffraction limited, so a pinhole was placed at the focal plane to select only the Airy disk diameter for the power measurements. As the point spread function and encircled energy plots in Figure 16

indicate, optical performance of the lenses is comparable. A pinhole with a diameter of 50 microns was selected to be used for these measurements.

(a)

(b)

(c)

(d)

Figure 16. (a) Point spread function of the reference refractive lens, (b) Encircled energy plot of the reference refractive lens, (c) PSF of the harmonic diffractive lens, and (d) Encircled energy plot of the harmonic diffractive element.

Figure 17 shows sample images of the focused spot with the lenses and with the pinhole acting as a filter to filter out only the Airy disk diameter.
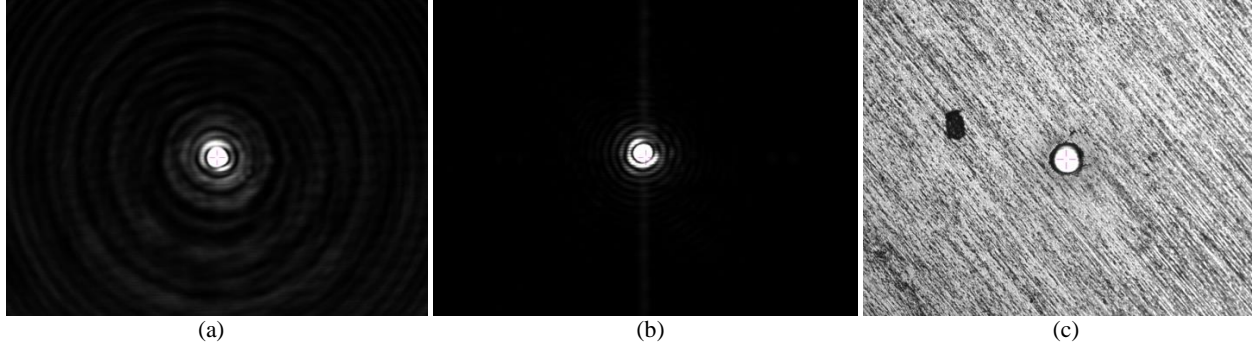
Figure 17. Image of the focused spot with (a) the harmonic diffractive lens at 810nm, (b) the reference refractive lens at 740nm, (c) with the 50 micron pinhole.

We used a tunable HeNe at wavelengths of 594nm, 604nm, 612nm, 633nm and a tunable Ti:Sapphire laser for measurements from 700nm to 1000nm in increments of 10nm. At wavelengths greater than 900nm, we observed fringes dominating the point spread function and placed a spatial filter to mitigate back reflections from the filter surfaces. A sample images illustrating the effects of fringes are shown in Figure 18. A plot of the measured diffraction efficiencies is shown in Figure 19 against the modeled efficiency curve. The measured efficiency peaks were about 90% and were all located near the expected wavelengths. The troughs in the measured diffraction efficiency were around the 40%~50% mark in the same wavelength range.
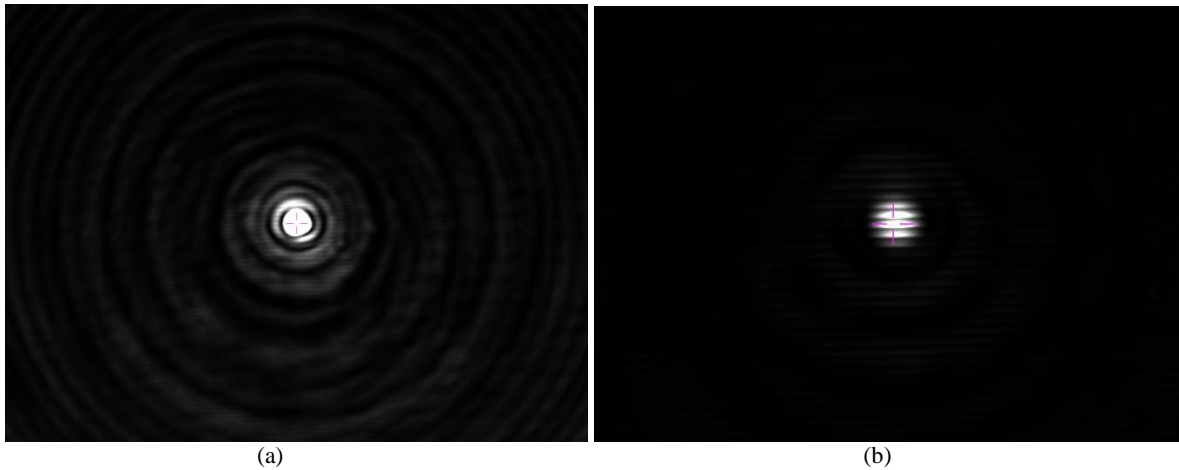
Figure 18. Image of focused spot with the harmonic DOE at (a) 810nm, and at (b) 900nm
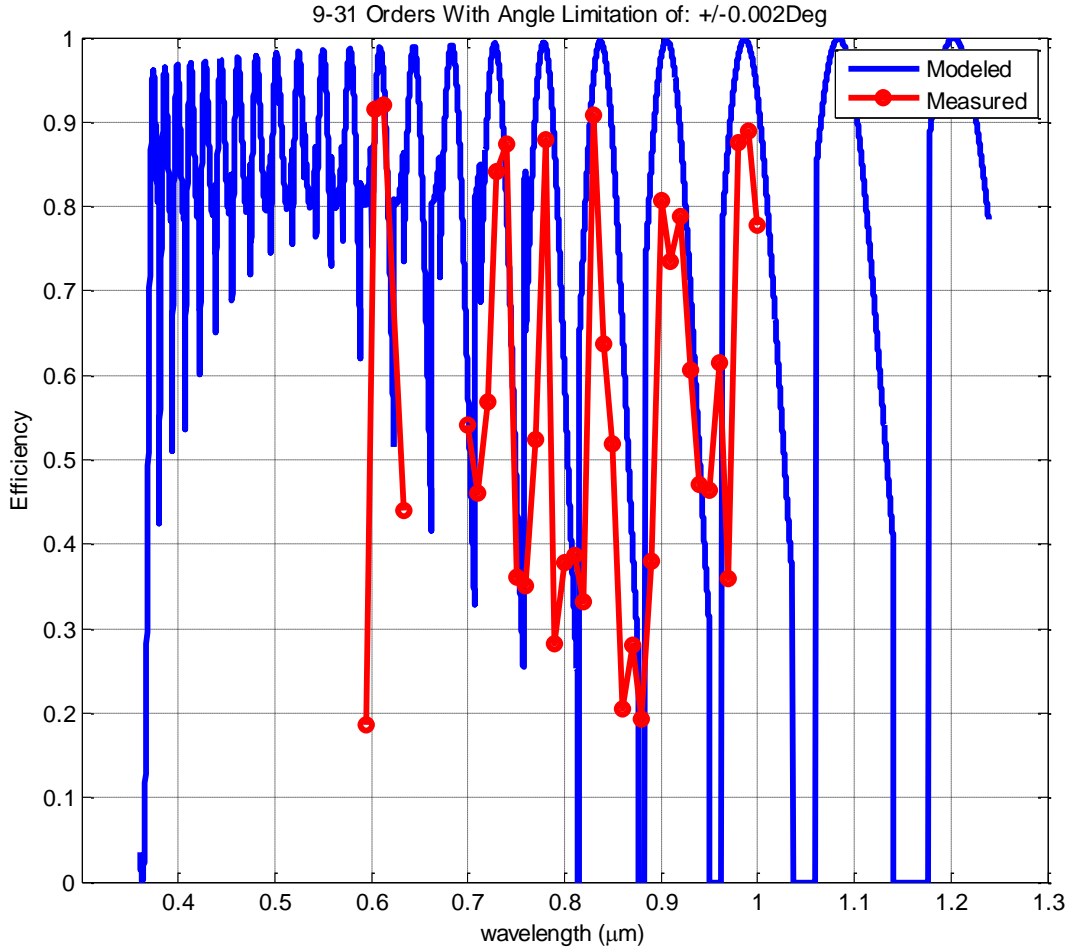
Figure 19. Plot of measured diffraction efficiency of the harmonic diffractive element. The measurement of the first group (0.594um to 0.633um) was done with a tunable HeNe laser while the second group (0.7um to 1.0um) was done with a tunable Ti:Sapphire laser.

4.2. Measured efficiency of the multi-layer diffractive element

Test setup for the multi-layer diffractive lens required an additional focusing lens as the multi-layer diffractive was an optically weak component as shown in Figure 20. In Figure 20, the first optical element on the left is the focusing lens and the two layers of diffractive components follow. As this test configuration is a non-ideal for diffractive elements with a converging incident beam, the system produced image quality comparable to a reference refractive lens.
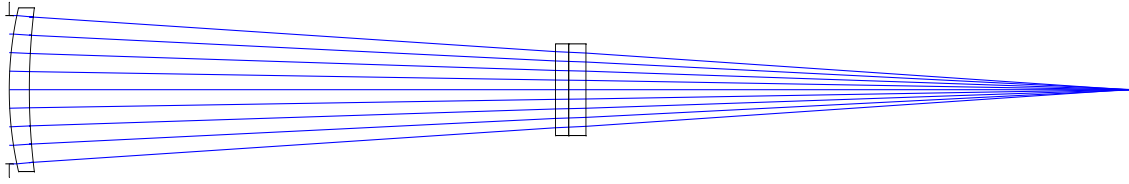
Figure 20. Diagram of the test setup for the multi-layer diffractive element.

Although both the test and the reference optics were limited by spherical aberration, both systems had about 85% of the energy within a 50um diameter. The PSF and encircled energy plots are shown in Figure 21.
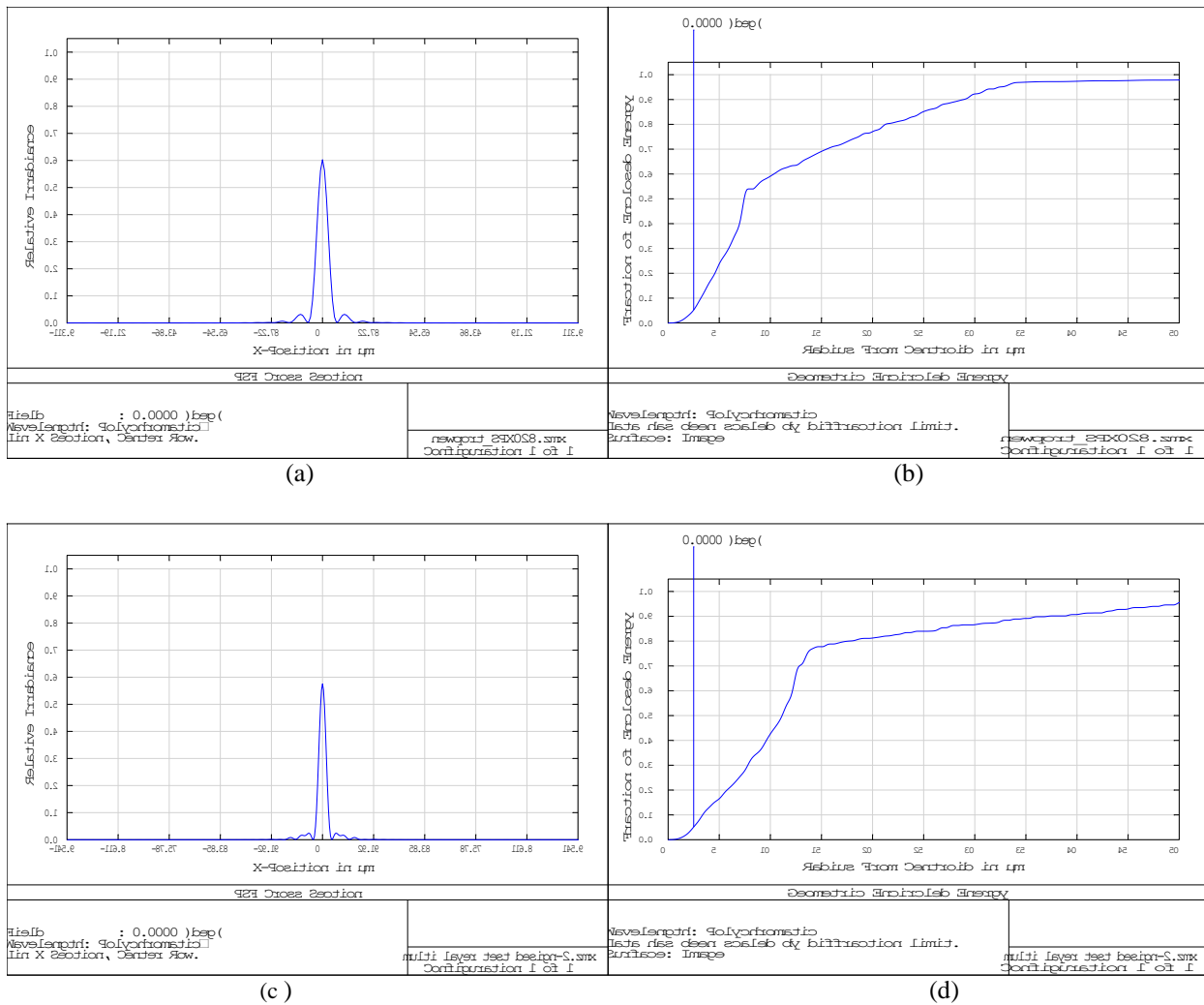
Figure 21. (a) Point spread function of the reference refractive lens, (b) Encircled energy plot of the reference refractive lens, (c) PSF of the multi-layer diffractive lens, and (d) Encircled energy plot of the multi-layer diffractive element.

Power measurements were made with a pinhole diameter of 50 microns using a tunable HeNe at the following five wavelengths: 543nm, 594nm, 604nm, 612nm, and 633nm. The measurement results are compared against model predictions in Figure 22. The diffraction efficiency model used in Figure 22 reflects the as-built etch depth values of 31.9 microns for the calcium fluoride element and 29.2 microns for the fused silica optic. Another variable that affects the diffraction efficiency but was not captured in the model prediction was the angle of the incident beam. The model assumes a collimated beam but the measurement was with a converging beam with a maximum ray angle of 3.3 degrees.
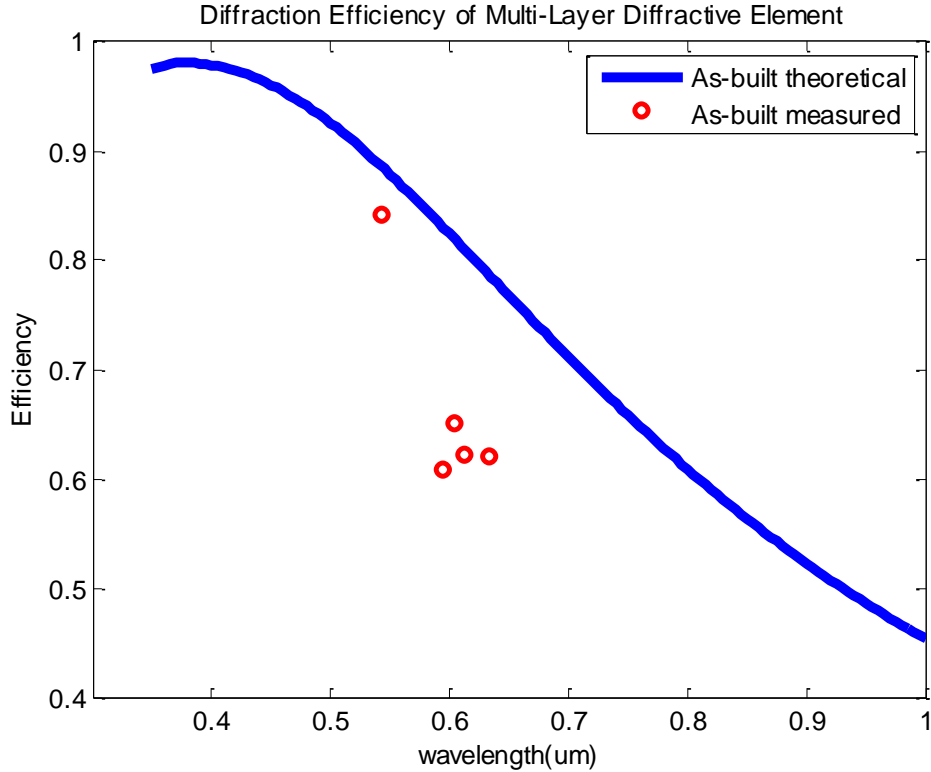
Figure 22. Plot of measured diffraction efficiency of the multi-layer diffractive element. The measurement was done with a tunable HeNe laser.

5. CONCLUSIONS

Diffractive optical elements have the potential to expand the design trade-space for optical systems by reducing the size, weight, and complexity of optical systems. However, conventional diffractive elements are limited in the working spectral bandwidth and Sandia lacked the modeling competency for broadband diffractive elements.

We have developed diffraction efficiency modeling tools and utilized them to design, fabricate, and test two extended spectral efficiency diffractive elements. One design involved two complementary diffractive elements made with different materials and the other was a single

component harmonic diffractive element. Both designs required deeper than conventional step heights approaching fabrication limitations for such designs using fused silica and calcium fluoride. The diffraction efficiency of the diffractive elements was measured by comparing power at the focused spot against a reference refractive lens at various wavelengths. The results for the harmonic diffractive design showed peak efficiencies of approximately 90% and troughs of about 40%. The wavelengths where the measured efficiency peaked stayed within +/- 5% of modeled values. A greater deviation from its model was observed with the multi-layer diffractive lens, where the measurements were made at five wavelengths. The efficiency values were lower by as much as 15% but were off by only 4% at a wavelength closer to the designed peak.

The diffraction efficiency models we have developed for two broadband diffractive element designs showed great agreement with test results, especially near the efficiency peaks. However, the model could be enhanced to include effects of optical coatings and new models could be developed to include off-axis illumination.

6. REFERENCES

[1] Kleemann, B.H., Seesselberg, M., Ruoff, J., Design concepts for broadband high-efficiecy DOEs. *Journal of the european optical society - rapid publications 3*, 08015 (april 2008), 1-16.

[2] Morris, G.M., Faklis D., Spectral properties of multiorder diffractive lenses. *Applied Optics*, 34, 14 (may 1995), 2462-2468.

[3] Davies, H., *Proc. Inst. Elec. Engrs.,* Vol 101, (1954), p.116

DISTRIBUTION

1	MS0406	Ron Baker	5712 (electronic copy)
1	MS0406	Junoh Choi	5712 (electronic copy)
1	MS0406	Anthony Tanbakuchi	5717 (electronic copy)
1	MS1139	Alvaro A. Cruz-Cabrera	1535 (electronic copy)
1	MS0359	D. Chavez, LDRD Office	1911 (electronic copy)
1	MS0899	Technical Library	9536 (electronic copy)

Sandia National Laboratories